

## Explaining key properties of lithiation in $\text{TiO}_2$ -anatase Li-ion battery electrodes using phase-field modeling

Niek J. J. de Klerk,<sup>1</sup> Alexandros Vasileiadis,<sup>1</sup> Raymond B. Smith,<sup>2</sup> Martin Z. Bazant,<sup>2,3</sup> and Marnix Wagemaker<sup>1,\*</sup>

<sup>1</sup>*Department of Radiation Science and Technology, Delft University of Technology, Mekelweg 15, 2629JB Delft, The Netherlands*

<sup>2</sup>*Department of Chemical Engineering, Massachusetts Institute of Technology, Cambridge, Massachusetts 02139, USA*

<sup>3</sup>*Department of Mathematics, Massachusetts Institute of Technology, Cambridge, Massachusetts 02139, USA*

(Received 5 April 2017; published 26 July 2017)

The improvement of Li-ion battery performance requires development of models that capture the essential physics and chemistry in Li-ion battery electrode materials. Phase-field modeling has recently been shown to have this ability, providing new opportunities to gain understanding of these complex systems. In this paper, a novel electrochemical phase-field model is presented that captures the thermodynamic and kinetic properties of lithium insertion in  $\text{TiO}_2$ -anatase, a well-known and intensively studied Li-ion battery electrode material. Using a linear combination of two regular solution models, the two phase transitions during lithiation are described as lithiation of two separate lattices with different physical properties. Previous elaborate experimental work on lithiated anatase  $\text{TiO}_2$  provides all parameters necessary for the phase-field simulations, giving the opportunity to gain fundamental insight in the lithiation of anatase and validate this phase-field model. The phase-field model captures the essential experimentally observed phenomena, rationalizing the impact of C rate, particle size, surface area, and the memory effect on the performance of anatase as a Li-ion battery electrode. Thereby a comprehensive physical picture of the lithiation of anatase  $\text{TiO}_2$  is provided. The results of the simulations demonstrate that the performance of anatase is limited by the formation of the poor Li-ion diffusion in the  $\text{Li}_1\text{TiO}_2$  phase at the surface of the particles. Unlike other electrode materials, the kinetic limitations of individual anatase particles limit the performance of full electrodes. Hence, rather than improving the ionic and electronic network in electrodes, improving the performance of anatase  $\text{TiO}_2$  electrodes requires preventing the formation of a blocking  $\text{Li}_1\text{TiO}_2$  phase at the surface of particles. Additionally, the qualitative agreement of the phase-field model, containing only parameters from literature, with a broad spectrum of experiments demonstrates the capabilities of phase-field models for understanding Li-ion electrode materials, and its promise for guiding the design of electrodes through a thorough understanding of material properties and their interactions.

DOI: [10.1103/PhysRevMaterials.1.025404](https://doi.org/10.1103/PhysRevMaterials.1.025404)

### I. INTRODUCTION

High-energy densities realized by Li-ion batteries have enabled mobile applications scaling from mobile phones, tablets, and laptops, up to electrical vehicles. The application of batteries in electric vehicles in particular has driven the demand for faster and more efficient electricity storage. Different mechanisms may limit battery performance [1–3]: the electronic wiring in the electrodes, ionic transport through the electrolyte, the charge transfer reaction, and the solid-state transport process. Which of these mechanisms is limiting depends on the applied current and the morphology of the electrodes [3]. To understand the complex interplay of the processes in batteries and to enable improved battery design, various models have been developed [4–10]. Using these models it is possible to design better battery management systems [4], decrease charging times [5], estimate the effect of side reactions on performance [6], and study what limits the performance of a battery [7].

The challenge for models describing batteries is taking into account microscopic processes, such as phase transitions and interfaces, in combination with macroscopic phenomena such as many-particle effects [11] and charge transport. The nonequilibrium conditions in complete electrodes will lead to

macroscopic gradients in diffusing species, and the associated potential gradients can change phase-transition kinetics, as has been demonstrated for  $\text{LiFePO}_4$  [11]. Even when a model is obtained which reasonably describes the processes, it often involves a number of unknown physical parameters, which require fitting to experimental data. Although this may result in an appropriate model for conditions similar to those of the fitted experimental data, extrapolation to other operating conditions is uncertain [2], making accurate model validation under different conditions vital.

The introduction of phase-field modeling to the battery field [9,12–14] has enabled accurate prediction of the phase transitions both in individual electrode particles and multiparticle systems [11] representing entire electrodes. This is computationally feasible because the phase-interface is taken implicitly into account [9], making it unnecessary to evaluate the phase transition kinetics in every position in an electrode particle. Using phase-field models for  $\text{LiFePO}_4$  the observed decreasing miscibility and spinodal gap in nanoparticles [15] has been explained [13,16], the observed transition from a first-order phase transition to a solid solution reaction at high overpotentials [17,18] has been predicted, and the transition from particle by particle to a concurrent mechanism was predicted [11] consistent with observations [19]. Recently, a three-dimensional phase-field model has been presented for  $\text{LiFePO}_4$  [16], and crack formation and the effects this causes have also been incorporated [20]. The phase-field method has also been used

\*m.wagemaker@tudelft.nl

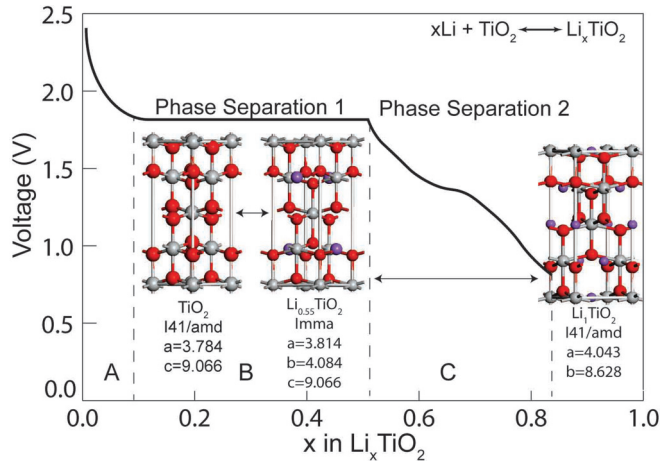


FIG. 1. The crystal structure [23] and typical voltage profile of anatase during lithiation.

to describe the lithiation of graphite electrodes [21,22], requiring the introduction of two first-order phase-transformations, which is relatively straight forward in a phase-field model, resulting in good agreement with experiments [21].

These results demonstrate the success of phase-field modeling of battery electrodes, and anatase  $\text{TiO}_2$  is another ideal candidate for applying phase-field modeling. It has been extensively studied for more than two decades, in which all parameters required for the phase-field model have been measured experimentally. This will allow comparison of a parameter free phase-field model towards a broad range of experimental results available in literature. Anatase  $\text{TiO}_2$  is an attractive Li-ion battery electrode material, based on its cheap and abundant elements, high theoretical capacity of  $335 \text{ mAh g}^{-1}$ , small volume expansion during lithiation [23], and good electronic conductivity [24].

The  $\text{TiO}_2$ -anatase lattice consists of stacked one-dimensional zigzag chains of  $\text{TiO}_6$  octahedra sharing distorted edges, as shown in Fig. 1. This stacking leads to empty zigzag channels with octahedral and tetrahedral interstitial sites that can accommodate lithium. A typical voltage profile for lithiation of anatase is shown in Fig. 1. At low Li concentrations, a solid solution is formed (region A), the length of which depends on the particle size [25–27]. Past the solid solution limit phase separation occurs, reflected by the plateau in region B, where half of the octahedral sites are filled to form the Li-titanate phase ( $\text{Li}_{0.5}\text{TiO}_2$ ). This is followed by a pseudoplateau (region C) during which the remaining octahedral sites are filled, forming  $\text{Li}_1\text{TiO}_2$ . Even though this phase transition usually does not show a voltage plateau, it is reported to occur via a phase separation mechanism [26,28].

In bulk anatase, roughly 0.6 lithium per formula unit is reversibly inserted in most experiments [26,27], leading to capacities of approximately  $200 \text{ mAh g}^{-1}$ . However, many parameters have been shown to affect the capacity drastically, including the preparation method [29], removing water from the anatase crystals before assembling the battery [30], the atmosphere during annealing [31], the morphology of the crystals [32], and the cutoff potential used during cycling [33]. However, the most decisive factor appears to be the

particle size [26,27,34,35]. By nanosizing anatase particles the  $\text{Li}_1\text{TiO}_2$  phase can be obtained at room temperature, realizing the theoretical capacity of  $335 \text{ mAh g}^{-1}$  [23,34].

For bulk samples, complete lithiation via electrochemical experiments has been reported, but only when kinetic restrictions were removed, either by lithiating at  $120^\circ\text{C}$  [36,37], or by allowing the anatase electrode to equilibrate during GITT measurements [25,27]. Computational results also indicate that full lithiation is energetically favorable [28,38], and attribute the fact that experimentally only small particles can fully lithiate to the slow Li diffusion in the lithium rich phase ( $\text{Li}_x\text{TiO}_2$ ,  $x > 0.5$ ) [38,39], which has also been measured by NMR spectroscopy [40]. It has been suggested that the slow Li diffusion makes the  $\text{Li}_1\text{TiO}_2$  layer act as a blocking layer, preventing further lithiation [40].

Despite the large amount of research regarding anatase, a comprehensive explanation for its complex behavior during lithiation is absent. In the present study, a phase-field model free of fitted parameters for the lithiation of anatase  $\text{TiO}_2$  is presented, based on microscopic parameters from the literature, describing both first-order phase-transitions. The phase-field model for anatase consistently explains the experimentally observed phenomena, improving the understanding of  $\text{TiO}_2$ -anatase during Li intercalation, and shedding light on the limitations and possibilities for anatase as an electrode material. Considering that this is achieved with a model that only contains parameters from the literature, this provides important validation for the physical foundation of phase-field modeling, especially considering the complex behavior of anatase during lithiation. Furthermore, our work strengthens the background of simulating materials that undergo multiple phase transitions during lithiation, which poses a considerable challenge for conventional computational models.

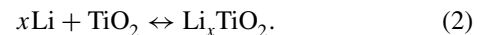
## II. PHASE-FIELD MODEL FOR ANATASE

In this section, the phase-field model for lithiation in anatase- $\text{TiO}_2$  is presented. For a thorough background on phase-field modeling the reader is referred to several comprehensive publications [9,41]. The most important macroscopic output variable for phase-field modeling of batteries is the measured cell voltage ( $V_{\text{cell}}$ ) given by

$$V_{\text{cell}} = -\Delta\mu/e + \eta_{\text{cell}}, \quad (1)$$

where  $\Delta\mu$  is the change in chemical potential,  $e$  the electron charge, and  $\eta_{\text{cell}}$  is the total cell overpotential.

The change in chemical potential is the difference in free energy of lithium at the solid-electrolyte interfaces of the anode and cathode material. For the simulated Li-metal/anatase system  $\Delta\mu$  is the change in free energy for the reaction:



Li metal is defined as the reference electrode, and consequently its chemical potential is defined as zero. Furthermore, the overpotential of the Li-metal electrode is assumed to be zero, which appears to be a good approximation given the small overpotentials experimentally observed for Li-metal electrodes [42]. These simplifications lead to a phase-field model in which only the lithiation of anatase needs to be taken into account to describe  $V_{\text{cell}}$ .

The two first-order phase-transitions occurring upon lithiation of anatase can be considered as two independent chemical reactions, since (locally) the two reactions cannot occur simultaneously, and can therefore be described by two independent lattices having their own free energy functional. The first lattice represents the reaction  $\text{TiO}_2 + 0.5\text{Li}^+ + e^- \leftrightarrow \text{Li}_{0.5}\text{TiO}_2$ , and the second lattice represents the reaction  $\text{Li}_{0.5}\text{TiO}_2 + 0.5\text{Li}^+ + e^- \leftrightarrow \text{Li}_1\text{TiO}_2$ . Similar to the phase-field model for graphite [43] this requires the introduction of two parameters ( $c_1$  and  $c_2$ ) that describe the Li concentration in the first and second lattice, respectively. In both lattices, the Gibbs free energy  $[g(\tilde{c}_i)]$  is described by a Cahn-Hilliard regular solution model [9]:

$$g(\tilde{c}_i) = k_B T (\tilde{c}_i \ln(\tilde{c}_i) + (1 - \tilde{c}_i) \ln(1 - \tilde{c}_i)) + \Omega_i \tilde{c}_i (1 - \tilde{c}_i) + \frac{1}{2} \frac{\kappa_i}{c_{\max}} |\nabla \tilde{c}_i|^2 + \tilde{c}_i \mu_i^\ominus, \quad (3)$$

where  $k_B$  is Boltzmann's constant,  $T$  the temperature in Kelvin,  $\tilde{c}_i$  the normalized concentration in lattice  $i$  ( $\tilde{c}_i = \frac{c_i}{c_{\max}}$ ),  $\Omega_i$  the enthalpy of mixing,  $\mu_i^\ominus$  the reference potential versus  $\text{Li}/\text{Li}^+$ , and  $\kappa_i$  the gradient penalty parameter.

The first term in Eq. (3) describes the entropy change upon adding Li ions ( $\tilde{c}_i$ ) and removing Li vacancies ( $1 - \tilde{c}_i$ ). The enthalpy of mixing ( $\Omega_i$ ) describes the interactions between Li atoms in an intercalation material. Positive values for  $\Omega_i$  correspond to attractive forces between Li atoms, favoring phase separation into the end member phase (a Li-rich and a Li-poor phases). The  $\kappa_i$  term represents the energy penalty for the existence of concentration gradients when phase-separation occurs, with larger values for  $\kappa_i$  leading to a wider interface region between Li-rich and Li-poor phases. Large entropy and  $\kappa_i$  terms in Eq. (3) promote solid solution behavior, while a large  $\Omega_i$  term will promote phase-separation. Which term dominates, and thus determines the phase behavior of a material, not only depends on the values of the parameters, but also on C rate, temperature, and particle size [3,17,44,45].

The diffusional chemical potential ( $\mu_i$ ) of lithium in anatase is given by the variational derivative of the free energy with respect to concentration [41]:

$$\mu_i = \frac{\partial g_i}{\partial \tilde{c}_i} - \nabla \cdot \frac{\partial g_i}{\partial \nabla \tilde{c}_i}. \quad (4)$$

Using Eq. (3), this gives

$$\mu_i = k_B T \ln \left( \frac{\tilde{c}_i}{1 - \tilde{c}_i} \right) + \Omega_i (1 - 2\tilde{c}_i) - \frac{\kappa_i}{c_{\max}} \nabla^2 \tilde{c}_i + \mu_i^\ominus. \quad (5)$$

From the diffusional chemical potential the flux of lithium ( $F_i$ ) through the particle can be determined based on the gradient of the diffusional chemical potential ( $\nabla \mu_i$ ) [9]:

$$F_i = -M_i c_i \nabla \mu_i = -\frac{D_i c_{\max} \tilde{c}_i}{k_B T} \nabla \mu_i, \quad (6)$$

where  $M_i$  is the mobility and  $D_i$  is the tracer diffusivity.

It is known that the lithium diffusion in  $\text{TiO}_2$ -anatase is dependent on the lithium concentration, but the effect of the Li concentration on Li diffusion is unclear. Papers with calculations show contradicting results, with some reporting a large [38] or small [46] increase in activation energy for

Li diffusion with increasing Li concentration, while others show a large [47] or small [39] decrease in activation energy at higher Li contents. Experiments by Sussman *et al.* [48] show a decrease in Li diffusivity with increasing Li content, although the magnitude of this effect strongly depends on the synthesis procedure. The simplest approximation for the tracer diffusivity on a lattice is proportional to the vacancy concentration,  $D_i \sim (1 - c_i)$ , in order to account for site exclusion [9,14] and for thermodynamic consistency with binary species mixing [49], but we find that this model is not able to reproduce the general features of the experimental voltage profiles. On the other hand, *ab initio* calculations predict a much stronger concentration dependence, where the chemical diffusivity drops by many orders of magnitude between the  $\text{TiO}_2$ ,  $\text{Li}_{0.5}\text{TiO}_2$ , and  $\text{Li}_1\text{TiO}_2$  phases [38], thus indicating stronger cooperative diffusion barriers. As a first approximation of such effects, we introduce a simple power-law correction:

$$D_i = D_i^* \frac{(1 - \tilde{c}_i)}{\tilde{c}_i}, \quad (7)$$

where  $D_i^*$  is the reference tracer diffusivity in lattice  $i$  at  $c_i = 0.5$ . Despite the unphysical divergence at  $c_i = 0$ , the diffusivity effectively saturates at realistic values in our phase-field simulations, since the regular solution model only allows small, but finite, concentrations. Combining Eqs. (6) and (7), the flux of lithium is given by

$$F_i = -\frac{D_i^* c_{\max} (1 - \tilde{c}_i)}{k_B T} \nabla \mu_i, \quad (8)$$

which is simply proportional to the vacancy concentration. The implied chemical diffusivity  $D_i^{\text{chem}} = D_i^* \left( \frac{1 - \tilde{c}_i}{\tilde{c}_i} - 2\Omega_i (1 - \tilde{c}_i)^2 \right)$ , is negative in the spinodal regions of thermodynamic instability, while capturing the strongly decreasing trend across the solid solution phases [38], similar to the experiments of Sussman *et al.* [48]. We find that this model is also capable of providing a good fit of the experimental voltage profiles.

Using Eqs. (5) and (8) the behavior of lithium inside anatase particles can be described, but to determine the battery voltage and influx of lithium the charge-transfer reaction at the electrode-electrolyte interface must also be described. This can be done using the Butler-Volmer equation [41]:

$$I_i = \frac{k_0 n e (a_O a_e^n)^{1-\alpha} a_{R,i}^\alpha}{\gamma_i^\ddagger} \times \left[ \exp \left( -\frac{\alpha e \eta_{\text{eff},i}}{k_B T} \right) - \exp \left( \frac{(1-\alpha) e \eta_{\text{eff},i}}{k_B T} \right) \right], \quad (9)$$

where  $I_i$  is the current density in lattice  $i$ ,  $k_0$  the reaction rate constant per surface area of the particle,  $\alpha$  the reaction symmetry factor (assumed to be 0.5),  $n$  the number of electrons participating in the reaction (one in this case), and  $e$  the electronic charge.

The charge-transfer overpotential ( $\eta_{\text{eff},i}$ ) is defined as  $e \eta_{\text{eff},i} = \mu_{R,i} - \mu_O$ , where  $\mu_{R,i}$  (the chemical potential of the reduced state of Li) is obtained from Eq. (5),  $\mu_O$  (the chemical potential of the oxidized state of Li) depends on the Li concentration in the electrolyte ( $c_{\text{lyte}}$ ) and is approximated using a dilute electrolyte model as  $\mu_O = k_B T \ln(c_{\text{lyte}})$ . The activity of the oxidized state ( $a_O$ ) is equal to  $c_{\text{lyte}}$ , the activity

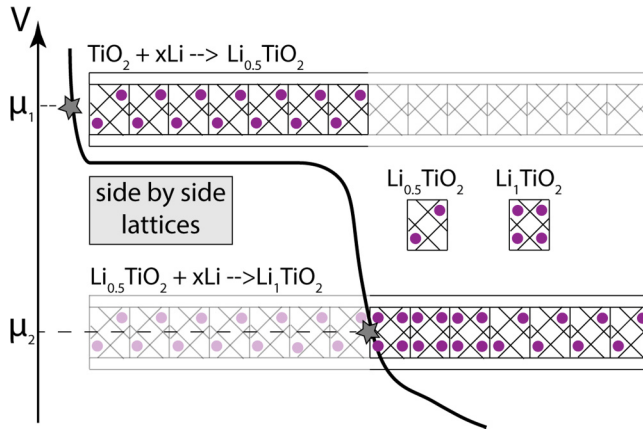


FIG. 2. Schematic representation of the two lattice phase-field model for lithiation in anatase  $\text{TiO}_2$ .

of the electrons  $a_e$  is taken to be unity. The activity of the reduced state ( $a_{R,i}$ ) depends on the diffusional chemical potential ( $\mu_i$ ) of lithium inside the particle:  $a_{R,i} = \exp(\frac{\mu_i - \mu_i^\ominus}{k_B T})$ , and the activity of the transition state ( $\gamma_i^\ddagger$ ) depends on the concentration of lithium vacancies [44]:  $\gamma_i^\ddagger = \frac{1}{1 - c_i}$ . During constant current simulations the applied current [ $I_{\text{applied}} = (I_1 + I_2) \times \text{Area}$ ] is known, thus  $\eta_{\text{eff},i}$  can be calculated.

The charge-transfer overpotential given by Eq. (9) describes the thermodynamic driving force for a lithium-ion to enter/leave the electrode particle. All the terms in Eq. (9) depend on the diffusional chemical potential or concentration of lithium, i.e., the size of the charge-transfer overpotential is determined by the Li concentration of the electrode and electrolyte near the electrode-electrolyte interface. Using the equations given above, the diffusional chemical potential of Li in the particles [Eq. (5)], the Li flow through the particle [Eq. (8)], and the Li flow into the anatase particles [Eq. (9)] can be described. Using the appropriate set of boundary conditions this set of equations can be solved [50], ultimately giving the cell voltage [Eq. (1)], and the Li concentration inside the anatase particles.

In contrast to the graphite phase-field model [21,22], which directly couples the two phase transitions, the anatase model consists of two independent lattices. The reason for this are the very different physical properties of the first and second phase transition in anatase, while in graphite the only difference

between the two phase transitions (relevant to the phase-field model) is the voltage. To describe the two phase transitions in anatase, different parameters are necessary, which can be implemented by introducing two independent lattices with different physical properties, schematically shown in Fig. 2. At the start of the lithiation process, the first phase transition will occur due to its higher intercalation potential, filling the first lattice with Li ions. When the first lattice fills, the charge-transfer overpotential will increase (lowering the voltage), because it gradually becomes harder to add more Li ions. When the intercalation potential of the second lattice is reached, lithiation of the second lattice becomes favorable, and the second phase transition will start. There are no interaction terms between the two lattices, since the effect the first lattice has on the second is already incorporated by the different parameters that are used. In Table I, all parameters and their values from literature are listed, as well as what each one is based on.

Normally, several physical parameters necessary for phase-field modeling are not available, either experimentally or computationally, and are therefore fitted by optimizing the phase-field model towards experimental voltage profiles. Intensive research towards lithiation of anatase  $\text{TiO}_2$  during the last decades makes it possible to quantify all parameters necessary for the present phase-field model. Thus providing a unique opportunity to validate a phase-field model, using only parameters from the literature, with micro- and macroscopic observations.

The reference potentials  $\mu_1^\ominus$  and  $\mu_2^\ominus$  are based on literature data which are closest to equilibrium conditions at room temperature.  $\mu_1^\ominus$  is based on GITT measurements [25,27] performed at room temperature, but for the second phase transition, equilibrium is not even reached during the reported GITT measurements. Therefore the value for  $\mu_2^\ominus$  is taken from experiments performed at 120 °C, in which the second plateau indicates that equilibrium was reached [36,37].

For anatase electrodes, electrochemical experiments have reported diffusivities in the first lattice between  $5 \times 10^{-10}$  and  $4 \times 10^{-20} \text{ cm}^2 \text{ sec}^{-1}$  [48,51–53,57–60], and changes of two orders of magnitude during charging have been reported [48]. Furthermore, calculations on Li diffusion in anatase also show strongly differing results [38,39,46,47], and NMR experiments indicate that diffusion over the interface between the anatase and Li-titanate phases [61,62] is the limiting step. For the second lattice, no experimental value for the diffusivity has been reported, but NMR experiments [40] and

TABLE I. The values of the parameters and on what information they are based.

Parameter	Value	Units	Based on
$\mu_1^\ominus$	1.82	V	GITT experiments [25,27]
$\mu_2^\ominus$	1.56	V	Electrochemical experiments at 120 °C [36,37]
$D_1^*$	$1 \times 10^{-16}$	$\text{cm}^2 \text{ sec}^{-1}$	Electrochemical experiments [51–53]
$D_2^*$	$1 \times 10^{-17}$	$\text{cm}^2 \text{ sec}^{-1}$	Force-field molecular dynamics simulations [39]
$\Omega_1$	$0.6 \times 10^{-20}$	J/Li	DFT calculations [28,38]
$\Omega_2$	$1.6 \times 10^{-20}$	J/Li	DFT calculations [28,38]
$\kappa_1$	$5.3 \times 10^{-8}$	J/m	Phase diagram (see text) [26]
$\kappa_2$	$0.8 \times 10^{-8}$	J/m	Phase diagram (see text) [26]
$c_{\text{max}}$	$1.419 \times 10^{28}$	$\text{Li m}^{-3}$	Neutron diffraction [54]
$k_0$	0.049	$\text{A m}^{-2}$	NMR experiments [55], also see Ref. [56]



calculations [38,39] have shown that it is smaller than in the first lattice.

Given the large range of values in the literature for Li diffusion in  $\text{TiO}_2$ -anatase several values from the literature were used for testing, after which the simulated voltage profiles were compared to experimental ones. The best agreement with experiments was obtained using a value of  $1 \times 10^{-16} \text{ cm}^2 \text{ sec}^{-1}$  for  $D_1^*$ , which has been reported by several experimental studies [51–53]. For  $D_2^*$ , a value of  $1 \times 10^{-17} \text{ cm}^2 \text{ sec}^{-1}$  gave the best results, which is obtained from molecular dynamics simulations [39].

Since it is impossible to experimentally measure the enthalpy of mixing, the values for  $\Omega_1$  and  $\Omega_2$  are based on DFT calculations [28,38]; the values were determined by the difference between the convex hull and the configurational energies. Values of  $\kappa_1$  and  $\kappa_2$  are based on the particle size at which two phase coexistence inside a particle no longer occurs [26]. This means that for the radial 1D model presented here the interface width  $\lambda_i$  corresponds to half of the particle size [15], which gives interface widths of 25 and 6 nm for lattice 1 and 2, respectively. Using these interface widths,  $\kappa_i$  can be calculated using [9]

$$\kappa_i = \lambda_i^2 c_{\max} \Omega_i. \quad (10)$$

The maximum Li concentration ( $c_{\max}$ ) is calculated based on the four Li sites per unit cell upon complete lithiation and the volume [54] of the unit cell of  $\text{Li}_{0.5}\text{TiO}_2$  divided over the two lattices. There is a small volume change (3%) upon lithiation from  $\text{TiO}_2$  to  $\text{Li}_{0.5}\text{TiO}_2$ , but given that the volume differs by just 0.1% between  $\text{Li}_{0.5}\text{TiO}_2$  and  $\text{Li}_1\text{TiO}_2$ , the volume of  $\text{Li}_{0.5}\text{TiO}_2$  is the best approximation over the range of possible Li concentrations.

The equilibrium charge transfer constant  $k_0$  is typically not known because it is very hard to experimentally distinguish the Li reaction between electrolyte and electrode from other processes occurring simultaneously. However, using NMR, this has been shown to be possible by Ganapathy *et al.* [55], reporting  $k_0$  for the  $\text{Li}_{0.5}\text{TiO}_2$  phase, which is at present assumed to be representative for both lattices. Please note that physically the second phase transformation can only occur after the first phase transformation has happened (locally), and although this is not formally implemented in the model, the 0.26 V lower insertion potential satisfies this condition during the simulations. To keep the model simple, all properties of anatase were assumed to be isotropic, a reasonable assumption given the 3D-diffusion pathway [39] and small changes in lattice parameters upon lithiation [23]. During lithiation of anatase  $\text{TiO}_2$ , the interfaces with the Li-rich phase are predicted to occur along strain invariant planes [38]. For this reason it was assumed that the role of strain and of stress assisted diffusion can be neglected in the present 1D simulations.

The simulations were performed using a modified version of the publicly available MPET code [63], in which the coupled differential equations are solved using the DAE tools package [64]. A 1D model along the radial direction of the particles is used for the simulations, and unless stated otherwise, simulations were performed on a single particle with a radius of 20 nm, a C rate of 0.5C, a temperature of 298 K, and a cutoff voltage of 1 V versus  $\text{Li}/\text{Li}^+$ . For the single-particle simulations the Li concentration in the electrolyte was

assumed to be constant, in multiparticle simulations the dilute electrolyte model as implemented in the MPET code [41] was used to describe the Li concentration in the electrolyte.

### III. RESULTS

The results of the phase-field model for lithiation of anatase  $\text{TiO}_2$  are compared to a broad spectrum of experimental results available in literature. The aim here is qualitative validation of the phase-field model and understanding of the physical processes that determine the performance of anatase electrodes. A qualitative validation rather than a quantitative validation is motivated by the many experimental parameters that affect the performance of anatase electrodes, resulting in a wide distribution of performances, even for equivalent electrochemical conditions [29].

#### A. Impact of lithiation rate

Similar to other electrode materials the (dis)charge rate, expressed in the C rate [a 2C rate corresponds to (dis)charge of the full theoretical battery capacity in 1/2 hour, 1C in 1 hour, 0.5C in 2 hours, etc.] has a large impact on the voltage profile of anatase electrodes. Typically, the capacity drops by approximately 25% when going from cycling at 0.5C to 1C [60], and at higher C rates a significant drop of the plateau voltage is detected [65].

The drops in capacity and voltage with increasing lithiation rate are both consistently reflected in the simulated voltage profiles for a single anatase particle with a radius of 20 nm shown in Fig. 3(a). At 5C, the simulation leads to a maximum composition of  $\text{Li}_{0.45}\text{TiO}_2$ , increasing to  $\text{Li}_{0.7}\text{TiO}_2$  at 0.5C, and at 0.1C the anatase particle is almost completely lithiated. With increasing lithiation rate the increasing charge-transfer overpotential results in a voltage drop in Fig. 3(a), driven by limited Li transport away from the surface. The significant decrease in voltage upon increasing the current from 0.01C to 0.1C indicates poor Li-ion kinetics in anatase, in particular considering the small particle radius of 20 nm. Generally, 0.1C results in close to equilibrium conditions in most nanostructured electrode materials, whereas in anatase  $\text{TiO}_2$  Li-ion kinetics still restricts the capacity at this rate.

The large voltage drop at high C rates for the second voltage plateau indicates that the formation of the  $\text{Li}_1\text{TiO}_2$  phase limits the charge transport away from the surface, thus increasing the charge-transfer overpotential. An estimate for the time it takes a Li ion to reach the center of the particle can be obtained by calculating the characteristic diffusion time [66],  $t_D$ , defined as

$$t_D = \frac{R^2}{D}, \quad (11)$$

where  $R$  is the particle radius and  $D$  the diffusion constant. For a particle with a radius of 20 nm, the characteristic times for diffusion in the  $\text{Li}_{0.5}\text{TiO}_2$  and  $\text{Li}_1\text{TiO}_2$  are approximately  $4 \times 10^4$  and  $4 \times 10^5$  seconds, respectively. For the first voltage plateau, the phase transition towards  $\text{Li}_{0.5}\text{TiO}_2$ , this roughly corresponds to 0.1C. Therefore, at this rate, the entire voltage plateau associated with the first phase transition should be observed, consistent with Fig. 3(a).

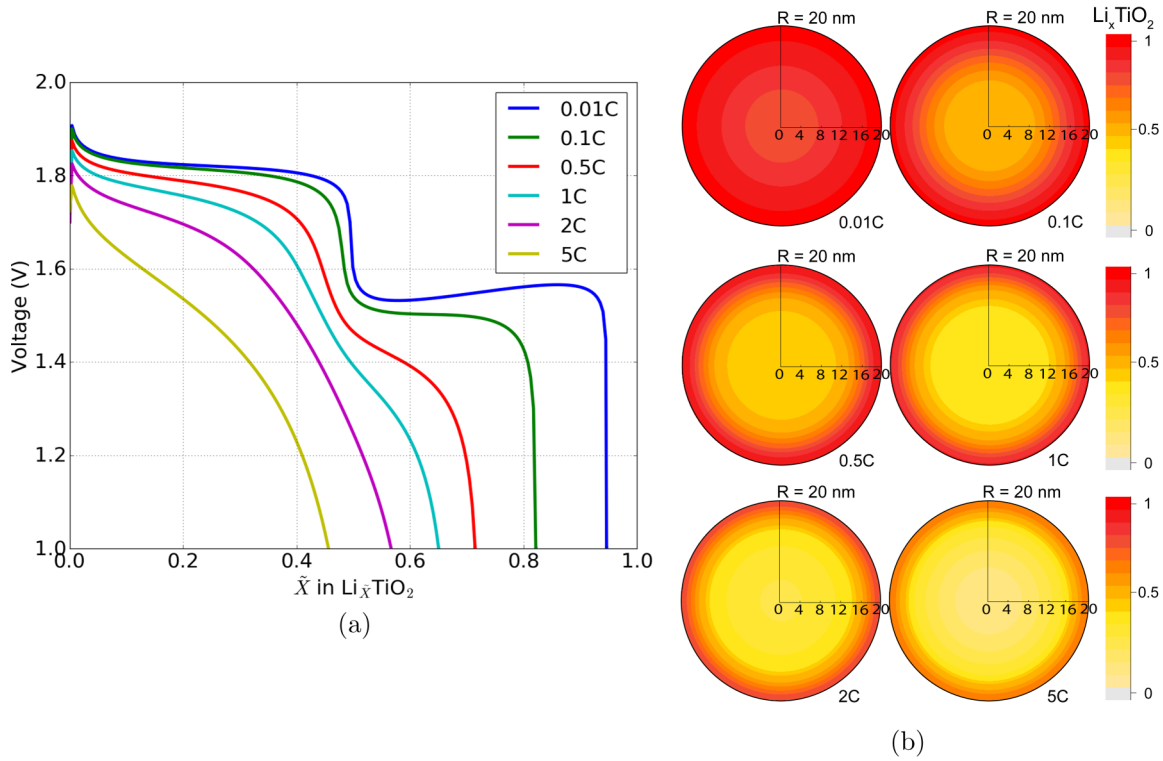


FIG. 3. (a) Voltages profiles vs average concentration ( $\bar{X}$ ) and (b) final concentration profiles in the particle at different C rates.

For the second voltage plateau, the phase transition towards  $\text{Li}_1\text{TiO}_2$ , the characteristic time roughly corresponds to 0.01C, consistently reflected by the complete appearance of the second voltage plateau at this C rate in Fig. 3(a). At time scales shorter than  $t_D$ , the lithium ions are unable to reach the center of the particle within the given time, i.e., kinetic limitations will restrict the capacity and decrease the cell voltage, as visible at higher C rates in Fig. 3(a). This is confirmed by the Li-ion concentration profiles shown in Fig. 3(b), in which at 0.01C most of the particles are transformed to the  $\text{Li}_1\text{TiO}_2$  phase. At 0.5C, only a thin layer at the surface approaches the maximum composition  $\text{Li}_1\text{TiO}_2$ , and the inner 10 nm is only transformed to the  $\text{Li}_{0.5}\text{TiO}_2$  phase. At 5C, this effect is augmented, with a large part of the particle having a Li concentration below  $x = 0.5$ , and only near the surface the Li concentration exceeds  $x = 0.5$ .

For experimental electrochemical lithiation at room temperature, only the onset of the second voltage plateau is observed, as consistently predicted by the simulation at 0.5C in Fig. 3(a). Raising the temperature to  $120^\circ\text{C}$  will significantly enhance Li diffusion, largely lifting the diffusional limitations of the second lattice, resulting in a clear experimental observation of the second voltage plateau at  $120^\circ\text{C}$  [36,37]. The simulation at a very slow lithiation rate, 0.01C, predicts that particles with a 20-nm radius can also be fully lithiated at room temperature. Although no experimental evidence showing this appears present (to the best of our knowledge), GITT measurements on particles with a diameter of 130 nm have been shown to reach full lithiation [25].

The increasing voltage at 0.01C is caused by simulating only a single particle. For a single particle the voltage follows the spinodal potential, giving an upwards slope in the voltage

profile [67]. When multiple particles are present interparticle phase-separation can occur, which smooths the voltage curve [21,67]. As demonstrated in Fig. S1 of Ref. [56] the upward tilt disappears when the simulations are performed on multiple particles.

In order to gain understanding of the rate limiting kinetic mechanism in anatase  $\text{TiO}_2$  electrodes, multiparticle simulations were performed. A  $50\text{-}\mu\text{m}$  porous electrode was separated into five volumes connected in series reflecting different depths inside the electrode, and each volume contained five particles with a  $20(\pm 2)\text{-nm}$  radius. The chosen rate is 2C, since at this rate the performance of the material already results in a significant decrease in the capacity and voltage, as shown in Fig. 3. The results of the multiparticle simulations in Fig. 4 demonstrate that the lithiation process proceeds concurrently at any given depth of the electrode. All particles are transforming simultaneously, which implies that the Li-ion diffusion in a single anatase grain is rate limiting, even when the particles are nano sized. In an actual electrode, the consequence is that all grains are actively participating in delivering the current, thus electrode performance can be improved significantly by increasing the Li diffusivity in the anatase lattice. For comparison, in the simulation shown in Fig. 4 the typical diffusion time ( $t_D$ ) through the electrolyte is 10 seconds (using an ambipolar diffusivity of  $2.5 \times 10^{-6} \text{ cm}^2 \text{ sec}^{-1}$ ), three orders of magnitude below the  $t_D$  inside the particles.

Furthermore, Singh *et al.* [24] have shown that  $\text{TiO}_2$  anatase without electron conducting additives has excellent cycling behavior. Thus electrode performance of  $\text{TiO}_2$  anatase can primarily be improved by increasing the Li diffusivity in the anatase lattice, and only slightly by enhancing the ionic and

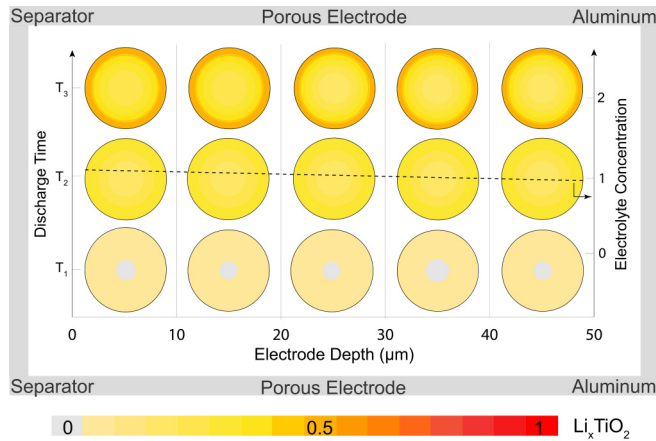


FIG. 4. Li-ion concentration profiles in the electrolyte and in electrode particles at different electrode depths at different times during 2C discharge. The filling fraction in the displayed particles is the average of that in the simulated particles in each volume.

electronic wiring. This behavior differs from other electrode materials, such as  $\text{LiFePO}_4$ ,  $\text{Li}_4\text{Ti}_5\text{O}_{12}$ , and  $\text{LiCoO}_2$ , where it has been shown that for full electrodes the ionic and electronic wiring dominate the internal resistance from small to large (dis)charge rates [68–72].

Interestingly, in  $\text{LiFePO}_4$ , the increasing overpotential when increasing the C rate widens the interface between the coexisting phases, at some critical rate leading to a solid-solution reaction as predicted by phase-field modeling [44] and observed experimentally [17–19]. In anatase  $\text{TiO}_2$  the phase interface also widens when increasing the C rate; however, even at large C rates, the  $\text{Li}_1\text{TiO}_2$  phase forms at the particle surface, because of the poor Li-ion diffusivity. Thus the model predicts that anatase  $\text{TiO}_2$  will undergo phase separation regardless of the imposed current.

### B. Impact of Li-diffusion coefficient

The impact of the C rate on the capacity and voltage for anatase  $\text{TiO}_2$  electrodes reveals that the Li-ion diffusivity in the anatase lattice is the key limiting factor. Experimentally, the Li diffusivity has been increased by annealing in argon [31], by hydrogen treatment [57], and by  $\text{Ti}^{3+}$  doping [73], which all increase the amount of oxygen vacancies in  $\text{TiO}_2$ . Impedance measurements have shown that this can increase the Li diffusivity by one order of magnitude [57]. To capture the effects of a higher Li diffusivity, simulations were performed at 0.5C and 2C, where the Li diffusion in both lattices is increased by a factor of 2, 5, and 10 compared to the values given in Table I.

As should be anticipated, this results in larger capacities and higher voltages with increasing diffusivity, as shown in Fig. 5, consistent with experimental observations [31,57,73]. For the lithium concentrations in the particle, the higher diffusivity results in an extension of the  $\text{Li}_1\text{TiO}_2$  phase from the surface of the particle. At 0.5C, the inside of the particle transforms completely to the  $\text{Li}_{0.5}\text{TiO}_2$  phase, even for the original diffusivity. While at 2C an increase of the diffusivity by a factor of 5 is necessary to transform the inside of the

particle to the  $\text{Li}_{0.5}\text{TiO}_2$  phase. These results confirm that increasing the diffusivity is a promising way to increase the capacity of anatase electrodes, especially when aiming at high (dis)charge rates.

### C. Impact of surface area

The simulations shown in Figs. 3 and 5 predict large charge-transfer overpotentials during the lithiation of anatase particles. These large overpotentials are caused by a high Li concentration near the surface of anatase particles, making it hard for Li ions to enter into the anatase particles. A reduction in the surface Li concentration can be achieved by increasing the surface area, which will lead to smaller charge-transfer overpotentials. An additional advantage is that a larger surface area also lowers the current density, which further decreases the charge-transfer overpotential.

This leads to larger capacities, as has been demonstrated by various experimental studies on high surface area anatase particles [74–76]. To capture the surface area effect simulations were performed on a spherical and a cylindrical particle (infinitely long, i.e., neglecting the top and bottom surface of the cylinder). The spherical particle has a surface to volume ratio of  $\frac{3}{R}$ , whereas the cylindrical particle has a smaller surface to volume ratio of  $\frac{2}{R}$ .

The concentration profiles in Fig. 6(b) show that when the cutoff voltage is reached, the Li concentration near the surface is comparable in the spherical and cylindrical particle. However, the larger surface area of the spherical particle allows for a larger Li-ion flux into the anatase  $\text{TiO}_2$  particle, resulting in a final Li fraction approximately 20% larger compared to the cylindrical particle. As shown in Fig. 6(a), at 0.5C, relatively small differences for the first voltage plateau are predicted, the difference in capacity being primarily caused by the second lattice. This is because the slower diffusion in the second phase leads to high Li concentrations near the surface more quickly, and thus high charge-transfer overpotentials at an earlier stage. Increasing the C rate to 2C significantly augments this effect, raising the difference in charge-transfer overpotential between the spherical and cylindrical particle, although the decrease in final Li composition is similar when compared to 0.5C.

Experimentally, similar observations are reported upon increasing the surface area [74–76]. However, higher surface areas are usually achieved by reducing the particle size [74,75], which has a similar impact on the voltage profiles, as shown in Fig. 7 and discussed below, making it hard to distinguish between the effects of nanosizing and particle shape.

### D. Impact of particle size

When Li-ion diffusion limits the electrode performance, decreasing the diffusion distance through the electrode material by particle size reduction is a well-established strategy to reach improved rate performance. Smaller particles increase the surface to volume ratio, which has been shown to be beneficial in the prior section. Additionally, particle size reduction has been shown to change the thermodynamics by increasing the solubility limits, which in small particles can even lead to suppression of phase separation, as shown for anatase  $\text{TiO}_2$  [26,77] and  $\text{LiFePO}_4$  [13,15].

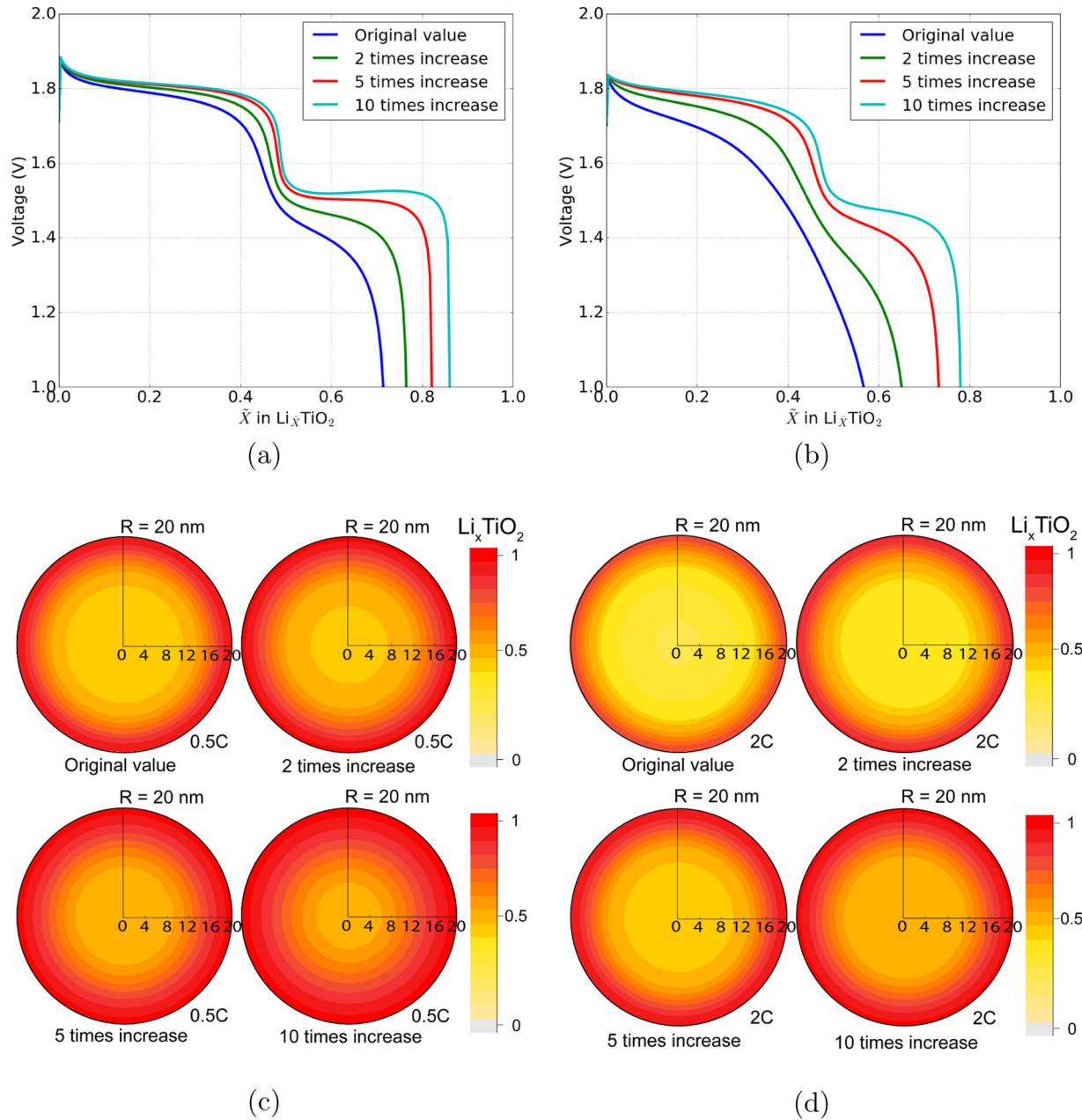


FIG. 5. Voltage profiles vs average concentration  $\bar{X}$  for different increases in diffusivity at (a) 0.5C, and (b) 2C, and final concentration profiles inside the particles at (c) 0.5C and (d) 2C.

A solid solution reaction can be expected to enhance Li-ion kinetics, in anatase specifically by suppressing the phase transition towards  $\text{Li}_1\text{TiO}_2$  at the particle surface, thereby promoting Li-ion transport and resulting in higher voltages and larger capacities at high C rates. Indeed, for anatase  $\text{TiO}_2$ , particle size reduction has been shown to improve performance drastically, for instance, resulting in complete lithiation of 7-nm particles at C/20 [23], whereas large particles cannot practically be lithiated to compositions exceeding  $\text{Li}_{0.6}\text{TiO}_2$  [26,34]. Consistently, phase-field simulations for different particle sizes, shown in Fig. 7, predict that decreasing the particle size diminishes kinetic limitations, resulting in nearly complete lithiation of 5 nm radius particles at 0.5C.

Experimentally, it has been reported that only the first few nanometres near the surface transform to the  $\text{Li}_1\text{TiO}_2$

phase [26,40,78], explaining why only nanoparticles are able to reach the theoretical  $\text{Li}_1\text{TiO}_2$  composition [23,26], and fully supported by the predicted concentration profiles in Fig. 8. At 0.5C and 2C, particles with a 5-nm radius transform completely to the  $\text{Li}_1\text{TiO}_2$  phase, while in bigger particles only the first few nanometres at the surface transform to the  $\text{Li}_1\text{TiO}_2$  phase. As a consequence, decreasing the particle size increases the capacity, in particular because of the increasing utilization of the second phase transition.

Increasing the C rate makes these effects more pronounced. For example, the final Li composition of the 50-nm-radius particle decreases from  $\text{Li}_{0.39}\text{TiO}_2$  to  $\text{Li}_{0.25}\text{TiO}_2$  when increasing the rate from 0.5C to 2C, while it only drops from  $\text{Li}_{0.98}\text{TiO}_2$  to  $\text{Li}_{0.94}\text{TiO}_2$  in the 5-nm particle. In the first place, improved performance upon particle size reduction can be



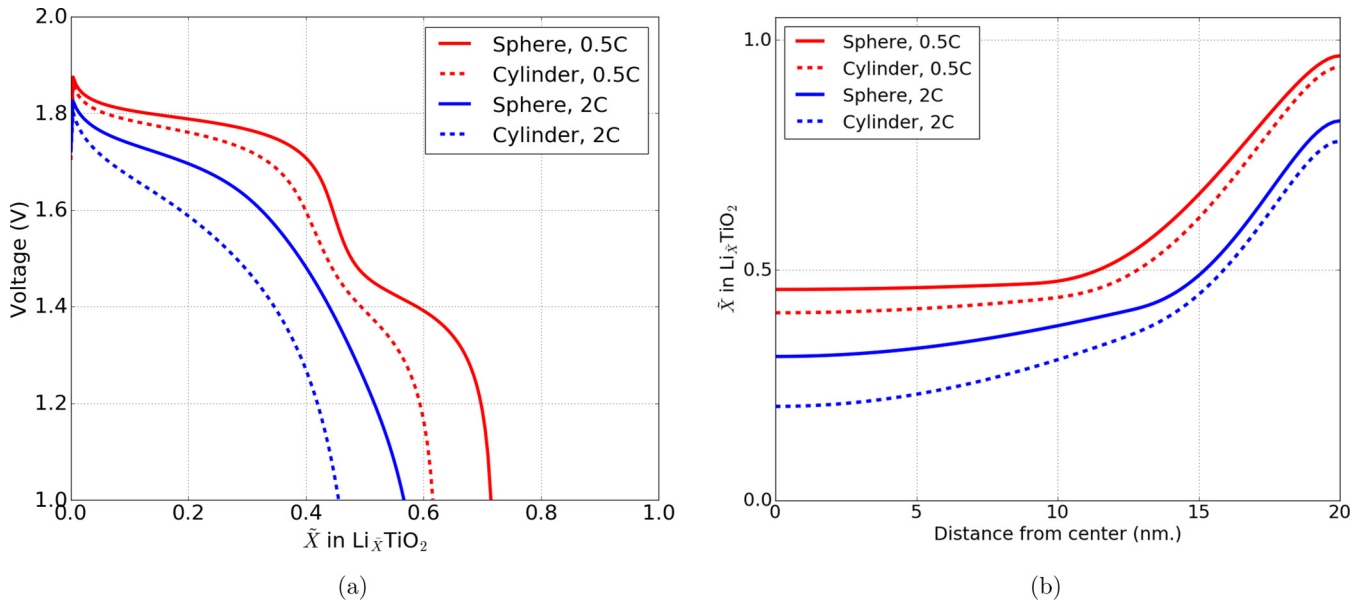


FIG. 6. (a) Voltage profiles vs average concentration  $\bar{X}$  and (b) final concentration profiles of a spherical and a cylindrical particle at 0.5C and 2C.

understood through the trivial effect of reducing the diffusion distance. The phase-field simulations also demonstrate that the nontrivial size effect, the destabilization of the first-order phase transition, plays a crucial role in the enhanced performance of the smaller particles. As shown in Fig. 10, the thickness of the  $\text{Li}_1\text{TiO}_2$  layer depends on the particle size, with smaller particles having thicker  $\text{Li}_1\text{TiO}_2$  layers. When the particle size approaches the width of the interface between the coexisting phases, phase separation is suppressed as previously shown for  $\text{LiFePO}_4$  [13,15].

For the  $\text{TiO}_2$ - $\text{Li}_{0.5}\text{TiO}_2$  and  $\text{Li}_{0.5}\text{TiO}_2$ - $\text{Li}_1\text{TiO}_2$  transitions, the interface widths are approximately 40 and 5 nm, respectively [26], directly related to the gradient penalty  $\kappa$ . This explains the evolution of the Li-ion concentration throughout

the 5- and 50-nm particles shown for 0.5C in Fig. 9. The 5-nm particle completely lithiates through a solid solution reaction in which both phase transitions are suppressed due to the small particle size. In the 50-nm particle, the first transformation from  $\text{TiO}_2$  to  $\text{Li}_{0.5}\text{TiO}_2$  is largely suppressed because it approaches the interface width of approximately 40 nm. However, at this particle size, the second transition from  $\text{Li}_{0.5}\text{TiO}_2$  to  $\text{Li}_1\text{TiO}_2$  is not suppressed.

The consequence of the particle size induced solid solution behavior is that the formation of the blocking  $\text{Li}_1\text{TiO}_2$  phase at the particle surface is prevented, as observed in Fig. 8, resulting in higher voltages and larger capacities for small particles. In larger particles, phase separation will occur, and Li concentrations near the surface will approach  $\text{Li}_1\text{TiO}_2$ . The

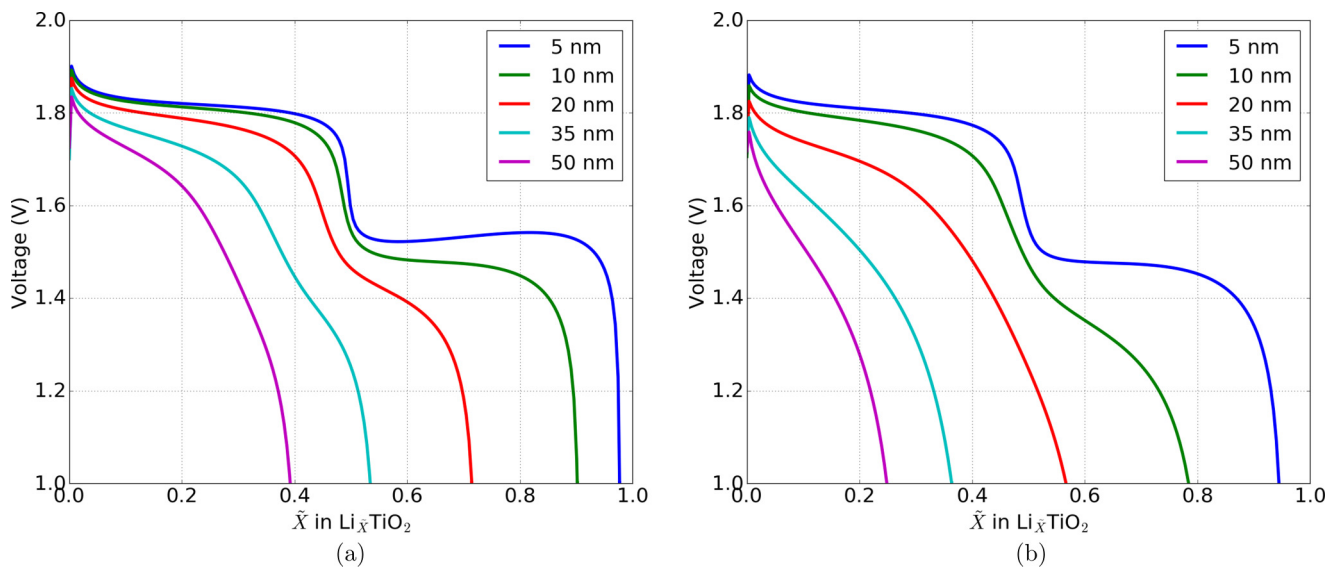


FIG. 7. Voltage profiles vs average concentration  $\bar{X}$  for particles with different radii at (a) 0.5C and (b) 2C.

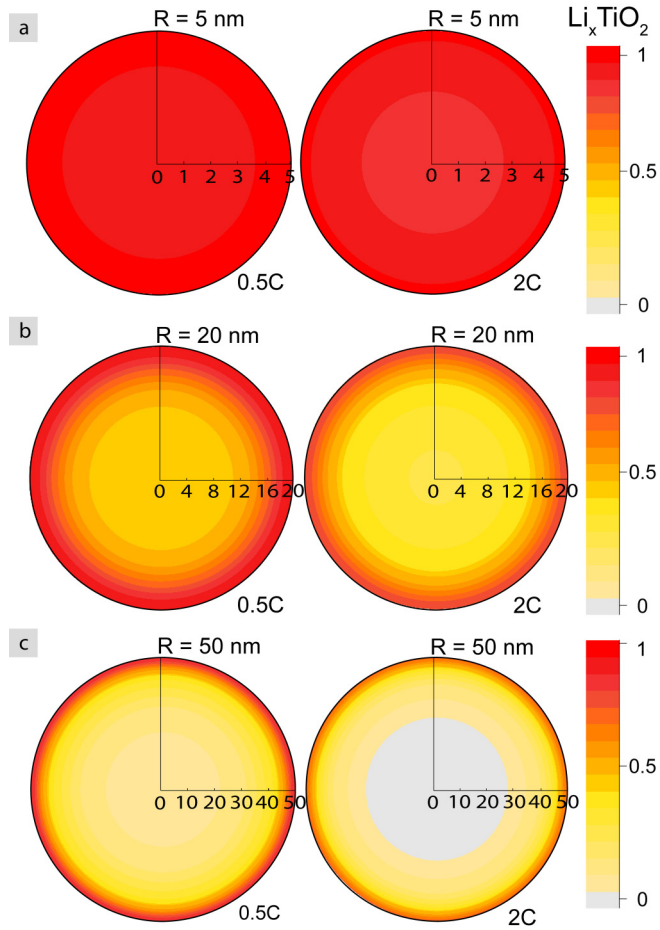


FIG. 8. Final concentration profiles at the end of a simulation at 0.5C and 2C for particles with a radius of (a) 5, (b) 20, and (c) 50 nm.

poor Li diffusivity in the  $\text{Li}_1\text{TiO}_2$  phase prevents moving of the phase boundary away from the surface, and the  $\text{Li}_1\text{TiO}_2$  surface layer will block further lithiation of the particle.

To show how this affects battery capacity, the final capacity versus C rate and final thickness of the  $\text{Li}_1\text{TiO}_2$ -layer versus C rate are shown for different particle sizes in Fig. 10. Figure 10 shows that the thickness of the blocking  $\text{Li}_1\text{TiO}_2$  layer strongly depends on the particle size and C rate, and that this is strongly correlated with the final capacity. As shown in Fig. 10, to obtain high capacities, small particles or low C rates are required, otherwise the layer of  $\text{Li}_1\text{TiO}_2$  forming at the surface will block Li intercalation. To obtain a general prediction of the maximum obtainable capacity as a function of applied current, the concept of Sand's time [79] could be used. However, to incorporate the nonlinear Li flux through the anatase particles, which also depends on the particle size, modifications to the formulation of Sand's time are necessary. For small particles, the simulations show good agreement with experiments, but for large particles ( $>35$  nm), the simulated maximum particle composition is significantly smaller than  $\text{Li}_{0.6}\text{TiO}_2$  at moderate C rates ( $>0.5\text{C}$ ), underestimating experimental observations [26,34]. We propose two arguments for this. First, in experiments, the surface area is larger compared to that of spherical particles assumed in the simulations. As a consequence the present simulations underestimate the amount of  $\text{Li}_1\text{TiO}_2$  formed, explaining the smaller capacities predicted. Second, although the phase-field calculations predict the extended solubility limits, the consequential enhanced Li-ion diffusivity is not implemented. Implementing this would require a diffusion term which depends on the local Li concentration and the gradient of the Li concentration, which requires further research outside of the scope of this study. Therefore the Li-ion diffusivity in particles where the solubility limits are

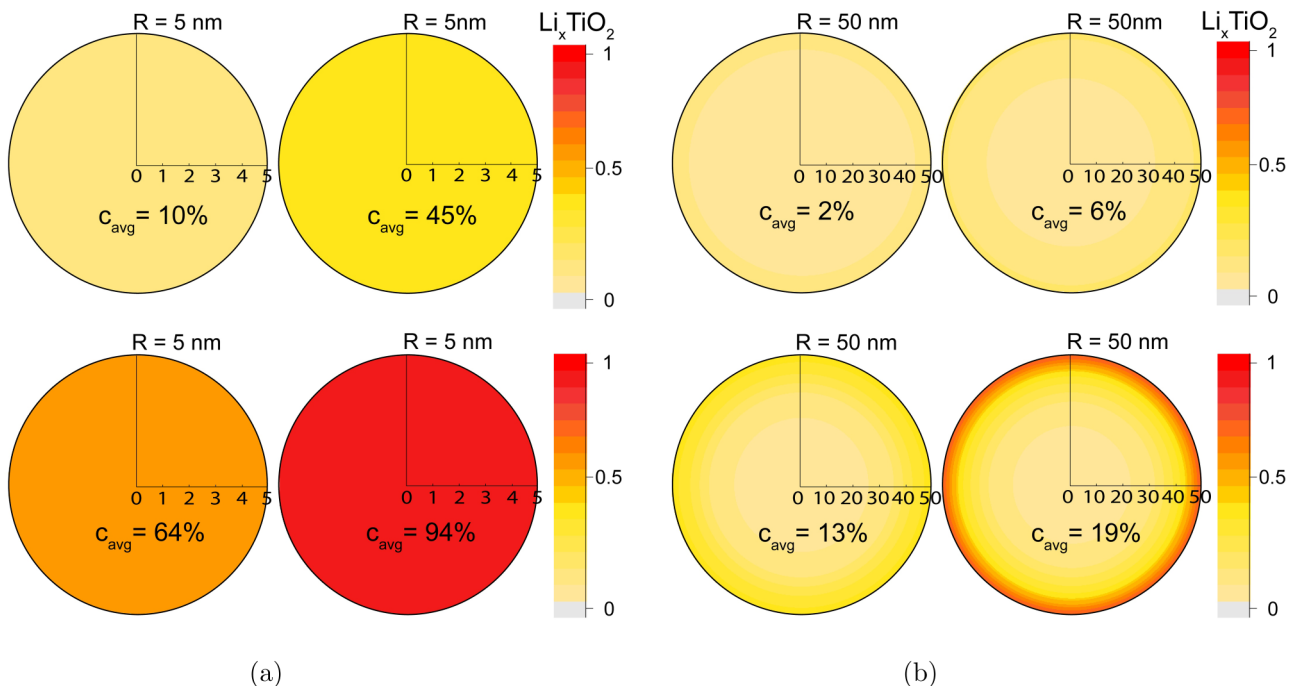


FIG. 9. Concentration profiles during a 0.5C simulation at different lithiation stages for particles with a radius of (a) 5 and (b) 50 nm.

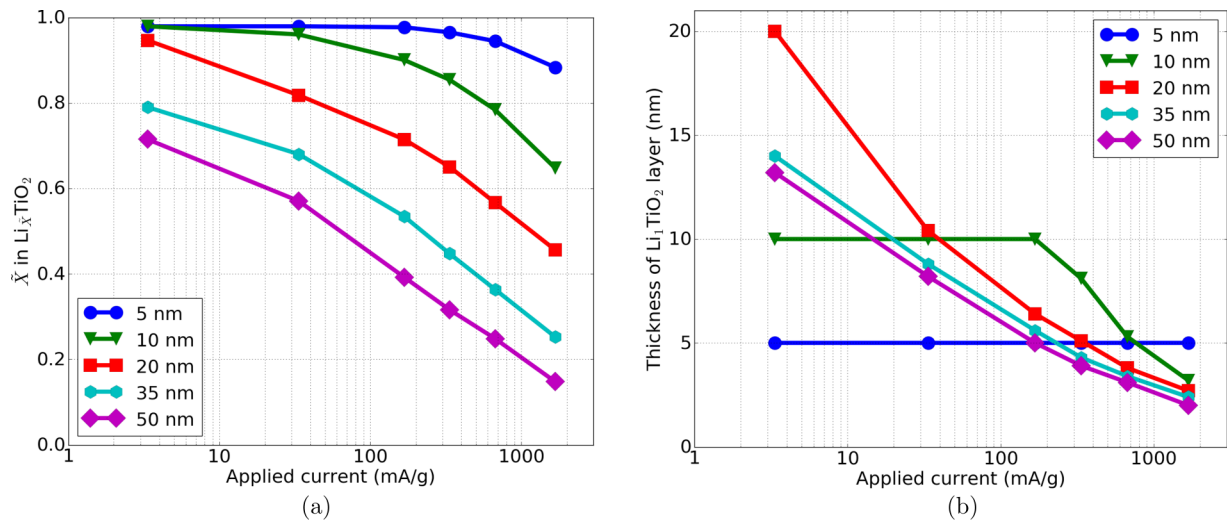


FIG. 10. For different particle sizes and C rates the (a) final Li concentrations and (b) final thickness of the  $\text{Li}_1\text{TiO}_2$  layer (defined as the depth at which  $\text{Li}_{0.6}\text{TiO}_2$  occurs), the lines are a guide to the eye.

significantly affected will be underestimated. This will be relevant for particle sizes comparable to the interface width, where in particular the larger interface width of the first phase transition enhances the Li-ion solubility limits. Thus explaining why for particles larger than 35 nm the present phase-field calculations underestimate the capacities as compared to experiments.

#### IV. DISCUSSION

As summarized in Fig. 11, the second phase transformation towards the  $\text{Li}_1\text{TiO}_2$  phase at the surface of anatase  $\text{TiO}_2$  particles is primarily responsible for the performance of anatase as Li-ion battery electrode. During lithiation,  $\text{TiO}_2$ -anatase is transformed to  $\text{Li}_{0.5}\text{TiO}_2$ , and this is followed by the formation of a thin layer of  $\text{Li}_1\text{TiO}_2$  at the particle surface. Because the Li diffusion is poor in the  $\text{Li}_1\text{TiO}_2$  layer, the thickness of this layer primarily depends on the applied C rate, as shown in Fig. 10.

When applying small C rates, the entire anatase particle is able to transform to the  $\text{Li}_1\text{TiO}_2$  phase, electrochemically

represented by a second voltage plateau. At moderate C rates only the onset of the second plateau will occur, as consistently predicted by the present phase-field simulations. For large C rates and/or large anatase particles, the lower voltage will drive the formation of a thin layer of the  $\text{Li}_1\text{TiO}_2$  phase. The slow Li transport through this layer prevents transformation of the complete particle towards the  $\text{Li}_1\text{TiO}_2$  phase. This is the origin of the observed large charge-transfer overpotentials, causing a shortening of the first voltage plateau, followed by a sloped tail in the voltage profile, thus rationalizing the decreasing capacities with increasing lithiation rates and increasing particle size.

The strongly concentration-dependent Li diffusion provides an explanation of the memory effect observed for anatase electrodes [76], which presents itself through a decrease in the voltage in the charge cycle (lithiation) following upon an incomplete charge/discharge cycle. The memory effect is caused by particles that are not completely delithiated before they are lithiating again, and thus more regions with poor diffusivity will remain in comparison to a complete charge/discharge cycle. In the memory cycle, the regions with poor diffusion will increase the charge-transfer overpotential in comparison to completely delithiated particles, explaining the observed memory effect. The phase-field simulations show that the charge-transfer overpotential strongly depends on the applied C rate and the surface to volume ratio, explaining the experimental observations [76] of a larger memory effect at high C rates and with smaller surface to volume ratios.

The blocking mechanism through the  $\text{Li}_1\text{TiO}_2$  phase formation at the surface of anatase particles, as predicted by the present simulations, indicates that the single-grain lithiation limits the rate performance of complete electrodes. This is explicitly demonstrated by the multiparticle phase-field simulation, where all particles transform concurrently. All grains are active, implying that the electrode is unable to provide a higher current due to the single particle limitations. This is unlike other electrode materials, such as  $\text{LiFePO}_4$ ,  $\text{Li}_4\text{Ti}_5\text{O}_{12}$ , and  $\text{LiCoO}_2$ , in which ionic and electronic wiring dominate the internal resistance [68–72]. The phase-field

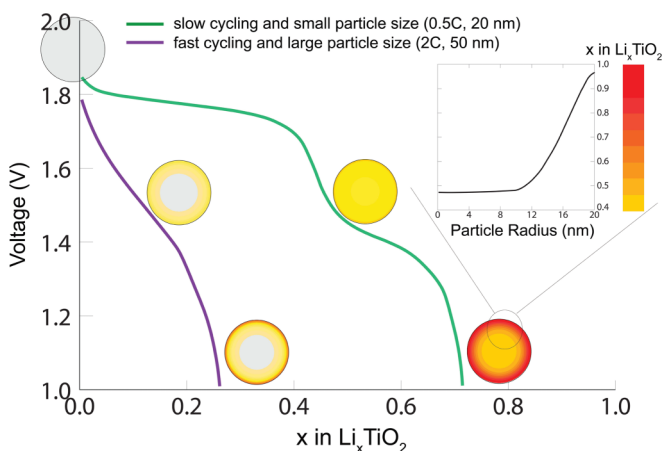


FIG. 11. Overview of Li intercalation in anatase.

model predicts that the applied overpotential is unable to induce solid solution behavior through widening of the phase interface regions, which has been shown for  $\text{LiFePO}_4$  [17], because at high overpotentials a layer of  $\text{Li}_1\text{TiO}_2$  phase will form at the surface, after which the poor Li-ion diffusivity in this phase consumes the applied overpotential.

## V. CONCLUSIONS

The present phase-field model with parameters from literature is able to qualitatively explain practically all experimental phenomena observed during lithiation of anatase electrodes. This includes the impact of particle size, C rate, Li-ion diffusivity, surface area, and the observed memory effect. The kinetic restrictions of the  $\text{Li}_1\text{TiO}_2$  phase forming at the surface of anatase particles is the origin of the performance restrictions, and prevents fast transformation of anatase particles, even under high current. The simulations reveal that the transformation of single anatase particles limits the performance of the complete electrode, rather than the ionic and electronic wiring that appears to be rate limiting for other electrode materials. This demonstrates that the limitation of anatase can only be addressed if the formation of a blocking  $\text{Li}_1\text{TiO}_2$  layer can be suppressed. This can be achieved by particle size reduction, where the reduction of the Li-ion diffusion distance as well as the suppression of the phase transitions enhances the Li-ion transport, increasing the capacity at high C rates. A second

strategy is to improve the Li-ion diffusivity in the anatase  $\text{TiO}_2$  lattice by doping. The simulations give detailed insight on the impact of both approaches, providing a rational strategy towards improved performance. Thus a comprehensive model for lithiation of anatase  $\text{TiO}_2$  has been presented. The good agreement with literature provides deep insight into the lithiation mechanism of anatase, and validation of the physical description of the phase-field model. This further motivates developing phase-field models for electrode materials, which will provide fundamental understanding of the limitations of battery materials, necessary for the formulation of strategies towards improved battery materials, design, and performance.

## ACKNOWLEDGMENTS

The research leading to these results has received funding from the European Research Council under the European Union's Seventh Framework Programme (FP/2007-2013)/ERC Grant Agreement No. [307161] of M.W. Financial support from the Advanced Dutch Energy Materials (ADEM) program of the Dutch Ministry of Economic Affairs, Agriculture and Innovation is gratefully acknowledged. R.B.S. and M.Z.B. acknowledge partial support from Samsung-MIT Alliance and the D3BATT project of the Toyota Research Institute.

N.J.J.deK. and A.V. contributed equally to this work.

- 
- [1] D. Deng, *Energy Sci. Eng.* **3**, 385 (2015).  
 [2] A. A. Franco, *RSC Advances* **3**, 13027 (2013).  
 [3] X. Zhang, T. W. Verhallen, F. Labohm, and M. Wagemaker, *Adv. Energy Mater.* **5**, 1500498 (2015).  
 [4] P. H. L. Notten and D. L. Danilov, *Adv. Chem. Eng. Sci.* **04**, 62 (2014).  
 [5] T. T. Vo, X. Chen, W. Shen, and A. Kapoor, *J. Power Sources* **273**, 413 (2015).  
 [6] V. A. Sethuraman, V. Srinivasan, and J. Newman, *J. Electrochem. Soc.* **160**, A394 (2012).  
 [7] M. Landstorfer, S. Funken, and T. Jacob, *Phys. Chem. Chem. Phys.* **13**, 12817 (2011).  
 [8] S. Dargaville and T. W. Farrell, *Electrochim. Acta* **111**, 474 (2013).  
 [9] M. Z. Bazant, *Acc. Chem. Res.* **46**, 1144 (2013).  
 [10] A. Salvadori, D. Grazioli, and M. G. D. Geers, *Int. J. Solids Struct.* **59**, 90 (2015).  
 [11] Y. Li, F. El Gabaly, T. R. Ferguson, R. B. Smith, N. C. Bartelt, J. D. Sugar, K. R. Fenton, D. A. Cogswell, A. L. D. Kilcoyne, T. Tylliszczak, M. Z. Bazant, and W. C. Chueh, *Nat. Mater.* **13**, 1149 (2014).  
 [12] G. K. Singh, G. Ceder, and M. Z. Bazant, *Electrochim. Acta* **53**, 7599 (2008).  
 [13] D. Burch and M. Z. Bazant, *Nano Lett.* **9**, 3795 (2009).  
 [14] T. R. Ferguson and M. Z. Bazant, *J. Electrochem. Soc.* **159**, A1967 (2012).  
 [15] M. Wagemaker, D. P. Singh, W. J. H. Borghols, U. Lafont, L. Haverkate, V. K. Peterson, and F. M. Mulder, *J. Am. Chem. Soc.* **133**, 10222 (2011).  
 [16] M. J. Welland, D. Karpeyev, D. T. O'Connor, and O. Heinonen, *ACS Nano* **9**, 9757 (2015).  
 [17] X. Zhang, M. van Hulzen, D. P. Singh, A. Brownrigg, J. P. Wright, N. H. van Dijk, and M. Wagemaker, *Nano Lett.* **14**, 2279 (2014).  
 [18] H. Liu, F. C. Strobridge, O. J. Borkiewicz, K. M. Wiaderek, K. W. Chapman, P. J. Chupas, and C. P. Grey, *Science* **344**, 1252817 (2014).  
 [19] X. Zhang, M. van Hulzen, D. P. Singh, A. Brownrigg, J. P. Wright, N. H. van Dijk, and M. Wagemaker, *Nat. Commun.* **6**, 8333 (2015).  
 [20] D. T. O'Connor, M. J. Welland, W. Kam Liu, and P. W. Voorhees, *Modell. Simul. Mater. Sci. Eng.* **24**, 035020 (2016).  
 [21] T. R. Ferguson and M. Z. Bazant, *Electrochim. Acta* **146**, 89 (2014).  
 [22] Y. Guo, R. B. Smith, Z. Yu, D. K. Efetov, J. Wang, P. Kim, M. Z. Bazant, and L. E. Brus, *J. Phys. Chem. Lett.* **7**, 2151 (2016).  
 [23] U. Lafont, D. Carta, G. Mountjoy, A. V. Chadwick, and E. M. Kelder, *J. Phys. Chem. C* **114**, 1372 (2010).  
 [24] D. P. Singh, A. George, R. V. Kumar, J. E. ten Elshof, and M. Wagemaker, *J. Phys. Chem. C* **117**, 19809 (2013).  
 [25] K. Shen, H. Chen, F. Klaver, F. M. Mulder, and M. Wagemaker, *Chem. Mater.* **26**, 1608 (2014).  
 [26] M. Wagemaker, W. J. H. Borghols, and F. M. Mulder, *J. Am. Chem. Soc.* **129**, 4323 (2007).  
 [27] G. Sudant, E. Baudrin, D. Larcher, and J.-M. Tarascon, *J. Mater. Chem.* **15**, 1263 (2005).



- [28] B. J. Morgan and G. W. Watson, *J. Phys. Chem. Lett.* **2**, 1657 (2011).
- [29] M. Søndergaard, Y. Shen, A. Mamakhel, M. Marinaro, M. Wohlfahrt-Mehrens, K. Wonsyld, S. Dahl, and B. B. Iversen, *Chem. Mater.* **27**, 119 (2015).
- [30] E. Madej, F. La Mantia, B. Mei, S. Klink, M. Muhler, W. Schuhmann, and E. Ventosa, *J. Power Sources* **266**, 155 (2014).
- [31] Y. Wang, S. Liu, K. Huang, D. Fang, and S. Zhuang, *J. Solid State Electrochem.* **16**, 723 (2011).
- [32] C. H. Sun, X. H. Yang, J. S. Chen, Z. Li, X. W. Lou, C. Li, S. C. Smith, G. Q. Lu, and H. G. Yang, *Chem. Commun.* **46**, 6129 (2010).
- [33] E. Madej, E. Ventosa, S. Klink, W. Schuhmann, and F. La Mantia, *Phys. Chem. Chem. Phys.* **16**, 7939 (2014).
- [34] V. Gentili, S. Brutti, L. J. Hardwick, A. R. Armstrong, S. Panero, and P. G. Bruce, *Chem. Mater.* **24**, 4468 (2012).
- [35] A. K. Rai, L. T. Anh, J. Gim, V. Mathew, J. Kang, B. J. Paul, J. Song, and J. Kim, *Electrochim. Acta* **90**, 112 (2013).
- [36] B. Zachau-Christiansen, K. West, T. Jacobsen, and S. Atlung, *Solid State Ionics* **28**, 1176 (1988).
- [37] W. J. Macklin and R. J. Neat, *Solid State Ionics* **53**, 694 (1992).
- [38] A. A. Belak, Y. Wang, and A. Van der Ven, *Chem. Mater.* **24**, 2894 (2012).
- [39] H. Yildirim, J. Greeley, and S. K. R. S. Sankaranarayanan, *J. Phys. Chem. C* **115**, 15661 (2011).
- [40] W. J. H. Borghols, D. Lützenkirchen-Hecht, U. Haake, E. R. H. van Eck, F. M. Mulder, and M. Wagemaker, *Phys. Chem. Chem. Phys.* **11**, 5742 (2009).
- [41] R. B. Smith and M. Z. Bazant, *J. Electrochem. Soc.* **164**, E3291 (2017).
- [42] N. Munichandraiah, L. G. Scanlon, R. A. Marsh, B. Kumar, and A. K. Sircar, *J. Electroanal. Chem.* **379**, 495 (1994).
- [43] R. B. Smith, E. Khoo, and M. Z. Bazant, *J. Phys. Chem. C* **121**, 12505 (2017).
- [44] P. Bai, D. A. Cogswell, and M. Z. Bazant, *Nano Lett.* **11**, 4890 (2011).
- [45] W. J. Borghols, M. Wagemaker, U. Lafont, E. M. Kelder, and F. M. Mulder, *J. Am. Chem. Soc.* **131**, 17786 (2009).
- [46] S. Lunell, A. Stashans, L. Ojamäe, H. Lindström, and A. Hagfeldt, *J. Am. Chem. Soc.* **119**, 7374 (1997).
- [47] F. Tielens, M. Calatayud, A. Beltran, C. Minot, and J. Andres, *J. Electroanal. Chem.* **581**, 216 (2005).
- [48] M. J. Sussman, A. Yasin, and G. P. Demopoulos, *J. Power Sources* **272**, 58 (2014).
- [49] E. B. Nauman and D. Q. He, *Chem. Eng. Sci.* **56**, 1999 (2001).
- [50] Y. Zeng and M. Z. Bazant, *SIAM J. Appl. Math.* **74**, 980 (2014).
- [51] J. Wang, J. Polleux, J. Lim, and B. Dunn, *J. Phys. Chem. C* **111**, 14925 (2007).
- [52] S.-H. Kim and S.-Y. Choi, *J. Electroanal. Chem.* **744**, 45 (2015).
- [53] H. Lindstrom, S. Sodergren, A. Solbrand, H. Rensmo, J. Hjelm, A. Hagfeldt, and S. E. Lindquist, *J. Phys. Chem. B* **101**, 7717 (1997).
- [54] M. Wagemaker, G. J. Kearley, A. A. van Well, H. Mutka, and F. M. Mulder, *J. Am. Chem. Soc.* **125**, 840 (2003).
- [55] S. Ganapathy, E. R. van Eck, A. P. Kentgens, F. M. Mulder, and M. Wagemaker, *Chemistry* **17**, 14811 (2011).
- [56] See Supplemental Material at <http://link.aps.org/supplemental/10.1103/PhysRevMaterials.1.025404> for a description of the many particle effects at 0.01c, and a comparison between the minimal and maximum charge transfer coefficients obtained from experiments.
- [57] J.-Y. Shin, J. H. Joo, D. Samuelis, and J. Maier, *Chem. Mater.* **24**, 543 (2012).
- [58] L. Kavan, *J. Solid State Electrochem.* **18**, 2297 (2014).
- [59] Z. Wang, J. Sha, E. Liu, C. He, C. Shi, J. Li, and N. Zhao, *J. Mater. Chem. A* **2**, 8893 (2014).
- [60] X. Yang, Y. Yang, H. Hou, Y. Zhang, L. Fang, J. Chen, and X. Ji, *J. Phys. Chem. C* **119**, 3923 (2015).
- [61] M. Wagemaker, R. van de Krol, A. P. M. Kentgens, A. A. van Well, and F. M. Mulder, *J. Am. Chem. Soc.* **123**, 11454 (2001).
- [62] M. Wagemaker, A. P. M. Kentgens, and F. M. Mulder, *Nature (London)* **418**, 397 (2002).
- [63] R. B. Smith, <https://bitbucket.org/bazantgroup/mpet>
- [64] D. D. Nikolić, *Comp. Sci.* **2**, e54 (2016).
- [65] M. G. Kim, H. Kim, and J. Cho, *J. Electrochem. Soc.* **157**, A802 (2010).
- [66] P. G. Bruce, B. Scrosati, and J. M. Tarascon, *Angew. Chem. Int. Ed. Engl.* **47**, 2930 (2008).
- [67] B. Orvananos, H. C. Yu, A. Abdellahi, R. Malik, C. P. Grey, G. Ceder, and K. Thornton, *J. Electrochem. Soc.* **162**, A965 (2015).
- [68] Z. Liu, T. W. Verhallen, D. P. Singh, H. Wang, M. Wagemaker, and S. Barnett, *J. Power Sources* **324**, 358 (2016).
- [69] F. C. Strobridge, B. Orvananos, M. Croft, H.-C. Yu, R. Robert, H. Liu, Z. Zhong, T. Connolley, M. Drakopoulos, K. Thornton, and C. P. Grey, *Chem. Mater.* **27**, 2374 (2015).
- [70] Y. Li, S. Meyer, J. Lim, S. C. Lee, W. E. Gent, S. Marchesini, H. Krishnan, T. Tyliczszak, D. Shapiro, A. L. Kilcoyne, and W. C. Chueh, *Adv. Mater.* **27**, 6591 (2015).
- [71] D. P. Singh, F. M. Mulder, and M. Wagemaker, *Electrochem. Comm.* **35**, 124 (2013).
- [72] C. Kim, N. S. Norberg, C. T. Alexander, R. Kostecki, and J. Cabana, *Adv. Funct. Mater.* **23**, 1214 (2013).
- [73] Y. Ren, J. Li, and J. Yu, *Electrochim. Acta* **138**, 41 (2014).
- [74] J.-Y. Shin, D. Samuelis, and J. Maier, *Adv. Funct. Mater.* **21**, 3464 (2011).
- [75] E. Madej, S. Klink, W. Schuhmann, E. Ventosa, and F. La Mantia, *J. Power Sources* **297**, 140 (2015).
- [76] E. Madej, F. La Mantia, W. Schuhmann, and E. Ventosa, *Adv. Energy Mater.* **4**, 1400829 (2014).
- [77] M. Wagemaker, F. M. Mulder, and A. Van der Ven, *Adv. Mater.* **21**, 2703 (2009).
- [78] M. Wagemaker, D. Lützenkirchen-Hecht, A. A. van Well, and R. Frahm, *J. Phys. Chem. B* **108**, 12456 (2004).
- [79] P. Bai, J. Li, F. R. Brushett, and M. Z. Bazant, *Energy Environ. Sci.* **9**, 3221 (2016).